SDSS'Rio 2010 STABILITY AND DUCTILITY OF STEEL STRUCTURES
E. Batista, P. Vellasco, L. de Lima (Eds.)
Rio de Janeiro, Brazil, September 8 - 10, 2010

BUCKLING, POST-BUCKLING, COLLAPSE AND DESIGN OF TWO-SPAN COLD-FORMED STEEL BEAMS

Cilmar Basaglia and Dinar Camotim

Department of Civil Engineering and Architecture, ICIST/IST, Technical University of Lisbon, Portugal
e-mails: cbasaglia@civil.ist.utl.pt, dcamotim@civil.ist.utl.pt

Keywords: Cold-formed steel, Two-span continuous beam, Buckling, Post-buckling, Structural design

Abstract. *This paper reports the available results of an ongoing numerical investigation on the buckling, post-buckling, collapse and design of two-span cold-formed steel lipped channel beams subjected to uniformly distributed loads. The results presented and discussed are obtained through analyses based on Generalised Beam Theory (elastic buckling analyses) and shell finite element models (elastic and elastic-plastic post-buckling analyses up to collapse). Moreover, the ultimate loads obtained are used to establish preliminary guidelines concerning the design of continuous (multi-span) cold-formed steel beams failing in modes that combine local, distortional and global features. An approach based on the existing Direct Strength Method (DSM) expressions is followed and the comparison between the numerical and predicted ultimate loads makes it possible to draw some conclusions concerning the issues that must be addressed by a DSM design procedure for cold-formed continuous beams.*

1 INTRODUCTION

In order to adequately design and assess the structural efficiency of cold-formed steel (thin-walled) members one must acquire in-depth knowledge on their non-linear response, a complex task that requires evaluating buckling stresses and determining post-buckling equilibrium paths up to collapse (accounting for initial imperfections). Indeed, a fair amount of research work has been recently devoted to the development of efficient design rules for isolated thin-walled members. The most successful end product of this research activity was the increasingly popular "Direct Strength Method" (DSM) [1], already included in the current Australian/New Zealander (AS/NZS4600: 2005) and North American (NAS: AISI-S100-07) specifications for cold-formed steel structures.

In practice, many thin-walled structural members exhibit multiple spans (*e.g.*, secondary elements like purlins or side rails) and are often subjected to non-uniform bending moment diagrams that combine positive (sagging) and negative (hogging) regions, a feature making their buckling behaviour rather complex, as it often (i) combines local, distortional and global features and (ii) involves a fair amount of localisation (*e.g.*, the occurrence of local and/or distortional buckling in the vicinity of the intermediate supports, where there are significant moment gradients and very little restraint can be offered to the slender bottom/compressed flanges). Even so, it seems fair to say that it is still very scarce the amount of research on the buckling and post-buckling behaviours of thin-walled steel beams subjected to non-uniform bending moment diagrams, namely continuous beams. In this context, it is worth mentioning the recent works of (i) Camotim *et al.* [2], who used Generalised Beam Theory (GBT) to analyse the buckling behaviour of steel beams with distinct loadings and support conditions (including intermediate supports), and (ii) Yu and Schafer [3], who investigated the influence of a linear bending moment gradient on the distortional buckling and post-buckling behaviours of single-span cold-formed steel beams, and used their finding to examine and extend the DSM design procedure for such members.

The aim of this work is to present and discuss the results of an ongoing numerical investigation on the buckling, post-buckling, collapse and DSM design of two-span lipped channel beams. The numerical results presented were obtained through (i) GBT buckling analyses and (ii) elastic and elastic-plastic shell finite element (SFE) post-buckling analyses. In particular, some interesting conclusions are drawn on the features that must be incorporated in a DSM design procedure for this type of cold-formed steel members.

2 NUMERICAL INVESTIGATION: SCOPE, MODELLING AND RESULTS

The buckling, post-buckling and ultimate strength results presented next concerning the non-linear behaviour of simply supported two-span symmetric lipped channel beams (i) with the cross-section dimensions given in figure 1(a), (ii) having overall lengths of *4.0m* (B4), *8.0m* (B8) and *10.0m* (B10), and (i) acted by a uniformly distributed load applied along the shear centre axis, causing only (pre-buckling) major-axis bending (see fig. 1(b)). The beam end sections are locally/globally pinned and can warp freely, and the intermediate support restrains all in-plane cross-section displacements. The post-buckling analyses incorporate small-amplitude critical-mode initial imperfections and do not account for residual stresses.

Concerning the GBT and SFE analyses, the following modelling issues deserve to be mentioned:

(i) *GBT Cross-Section Discretisation*. Figure 2 shows the nodes considered in the lipped channel section. This cross-section discretisation leads to *17* deformation modes, which are *global* (**1**-**4**), *distortional* (**5**-**6**) and *local* (**7**-**17**) – figure 3 shows the in-plane configurations of those more relevant for the buckling analyses.

(ii) *GBT Member Discretisation*. The GBT equilibrium equations were solved using the beam finite element developed by Camotim *et al.* [2]. Each beam span was discretised into *20* finite elements for the three beams.

(iii) *SFE Discretisation*. The SFE analyses, performed in the code ANSYS [4], were based on beam discretisations into fine meshes of 4-node SHELL181 elements, as illustrated in figures 4(a_1), 4(b_1) and 4(c_1).

(iv) *Material Modelling*. The steel material behaviour was deemed either linear elastic (bucking and post-buckling analyses) or linear-elastic/perfectly-plastic with von Mises yield criterion (post-buckling analyses).

(v) *Initial Imperfections*. Critical-mode initial geometrical imperfections with amplitude equal to either *10%* of the wall thickness (local or distortional buckling) or *L/2000* (global buckling).

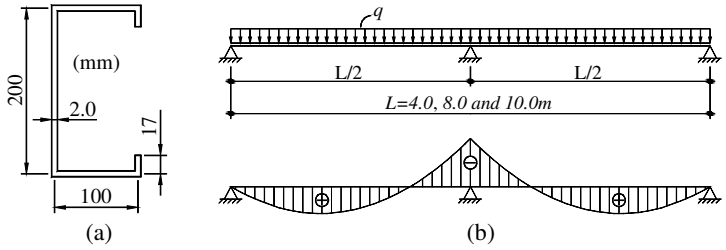

Figure 1: Two-span continuous beam (a) cross-section dimensions and (b) loading and first-order elastic bending moment diagram.

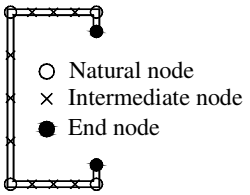

Figure 2: Lipped channel GBT discretisation.

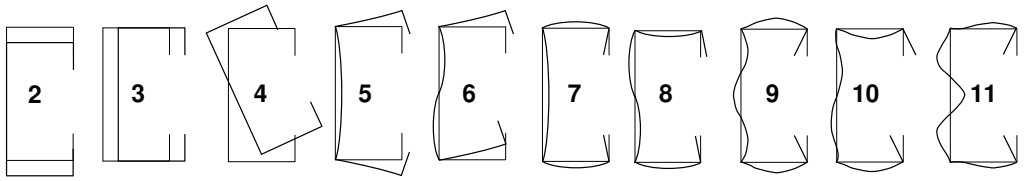

Figure 3: In plane shapes of the *10* most relevant lipped channel deformation modes.

2.1 Buckling Results

Figures 4(a_1)-(c_2) show the critical buckling mode shapes of the lipped channel B4, B8 and B10 beams – the left and right hand side figures are (i) ANSYS 3D views and (ii) GBT modal amplitude functions, respectively. The corresponding beam critical buckling loads, yielded by the GBT and ANSYS analyses, are (i) $q_{cr.GBT}$=*46.66kN/m* and $q_{cr.ANSYS}$=*46.78kN/m* (B4), (ii) $q_{cr.GBT}$=*10.82kN/m* and $q_{cr.ANSYS}$=*10.71kN/m* (B8), and (iii) $q_{cr.GBT}$=*6.06kN/m* and $q_{cr.ANSYS}$=*5.92kN/m* (B10). The analysis of these buckling results prompts the following remarks:

(i) The GBT and ANSYS critical buckling loads practically coincide – the maximum difference is *2.4%* and concerns the B10 beam, which buckles in a predominantly global mode. There is also very close agreement between the buckling mode shapes – this is particularly striking if one looks at the zoomed buckled

intermediate support regions shown in figures 4(a_1), (b_1) and (c_1).

(ii) The three beam critical buckling modes combine at least two types of deformation modes: (ii_1) local and distortional (B4), and (ii_2) local, distortional and global (B8 and B10).

(iii) Figure 4(a_2) shows that buckling involves only the B4 intermediate support region. The local modes **7**-**11** are dominant and the distortional modes **5**-**6** also play a relevant role (see the bottom flange rotation).

(iv) Figure 4(b_2) shows that the B8 buckling mode involves mostly the intermediate support region – there is a major contribution from the distortional modes **5**-**6** and also a non-negligible one from the local modes **7**-**8**. (note that it is quite difficult to detect the latter in the ANSYS output). The global modes **3**-**4** (minor axis bending and torsion) play a lesser role – their contributions are only meaningful within the beam spans.

(v) Figure 4(c_2) shows that the global modes **3**-**4** are highly dominant in the B10 buckling mode – they exhibit one half-wave per span with maximum participations at the middle. Moreover, there are small contributions of the local (**7**-**8**) and distortional (**5**-**6**) modes, but restricted to the close vicinity of the intermediate support.

It is worth noting that, in all existing design procedures, a crucial step is the identification of the buckling mode nature, which is by no means clear in the above three beams. In order to attempt to establish the "dominant nature" of these buckling modes, additional GBT analyses were carried out including only global (**2**-**4**), distortional (**5**-**6**) and local (**7**-**17**) deformation modes. Table 1 shows the relation between the "pure" global ($q_{b.e}$), distortional ($q_{b.d}$) and local ($q_{b.l}$) buckling loads and critical buckling load (q_{cr}), obtained with all the deformation modes – the "dominant buckling mode nature", indicated in the last column, reflects the "closeness" between the corresponding "pure" buckling load and q_{cr} (lowest of the three ratios), and obviously agrees with results shown in figure 4.

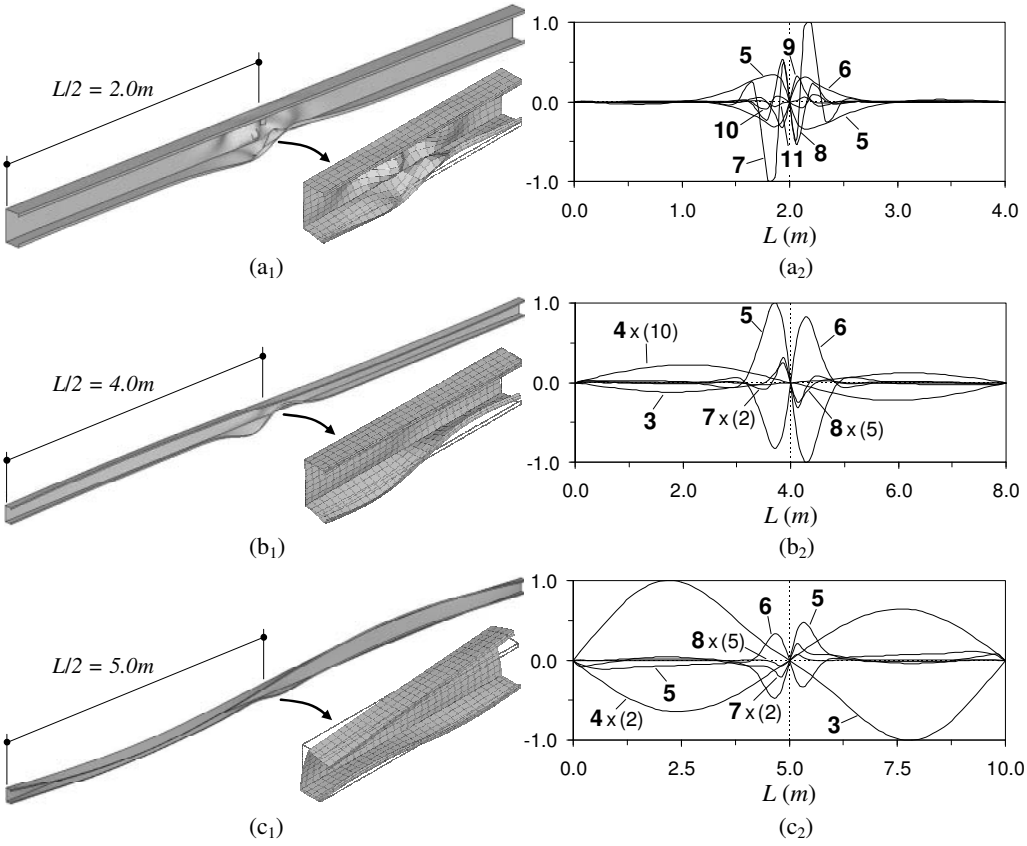

Figure 4: ANSYS and GBT-based buckling mode shapes of the (a_1)-(a_2) B4, (b_1)-(b_2) B8 and (c_1)-(c_2) B10 beams.

Table 1: Relation between q_b and q_{cr} load values.

Beam	$q_{b.e}/q_{cr}$	$q_{b.d}/q_{cr}$	$q_{b.l}/q_{cr}$	*Dominant buckling mode nature*
B4	5.193	1.399	1.032	Local
B8	1.439	1.104	1.187	Distortional
B10	1.074	1.172	1.391	Global

2.2 Post-Buckling Results

This section addresses the SFE analysis of the elastic and elastic-plastic (yield stresses f_y=*250,350,550,850MPa*) post-buckling behaviour of the B4, B8 and B10 beams. The curves shown in figures 5(a), 6(a) and 7(a) are the post-buckling equilibrium paths *q vs.* V_1, *q vs.* V_2 and *q vs.* V_3, where (i) the symbols □, △, ○ and ◇ indicate the ultimate loads and (ii) V_1, V_2 and V_3 are displacements selected to provide a better characterisation of the beam post-buckling behaviours – they correspond to the vertical displacements of the bottom flange-lip corner of cross-sections located in the beam left span and *23.4cm* (V_1) or *26.7cm* (V_2 and V_3) away from the intermediate support (see fig. 5(b)). Figure 5(c) concerns the B4 beam with f_y=*250MPa* and displays the deformed configurations and von Mises stress distributions associated with (i) the full yielding of the mid-cross-section (*i.e.*, the formation of the first beam plastic hinge) and (ii) the beam collapse. As for figures 6(b) and 7(b), they provide the failure mode and von Mises stress distributions of the B8 beam with f_y=*550MPa* and the B10 beam with f_y=*850MPa*, respectively.

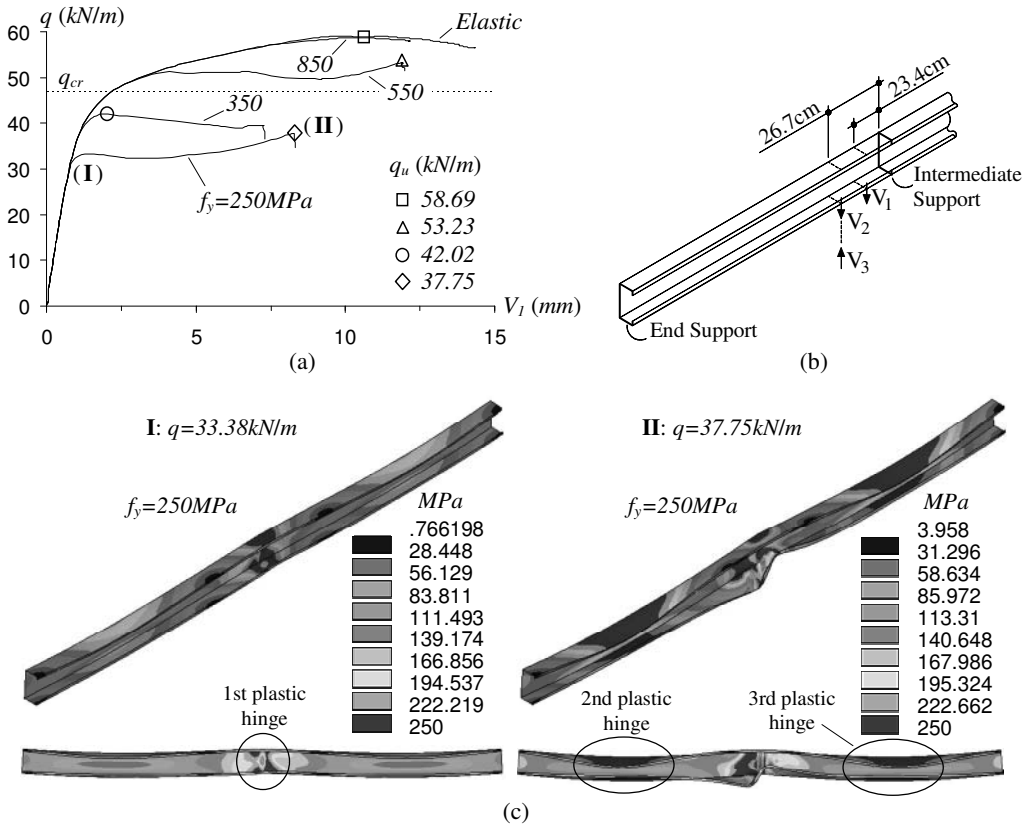

Figure 5: B4 beam (a) equilibrium paths, (b) location of the measured displacements and (c) deformed configuration and von Mises stresses associated with the formation of the first plastic hinge and at beam collapse.

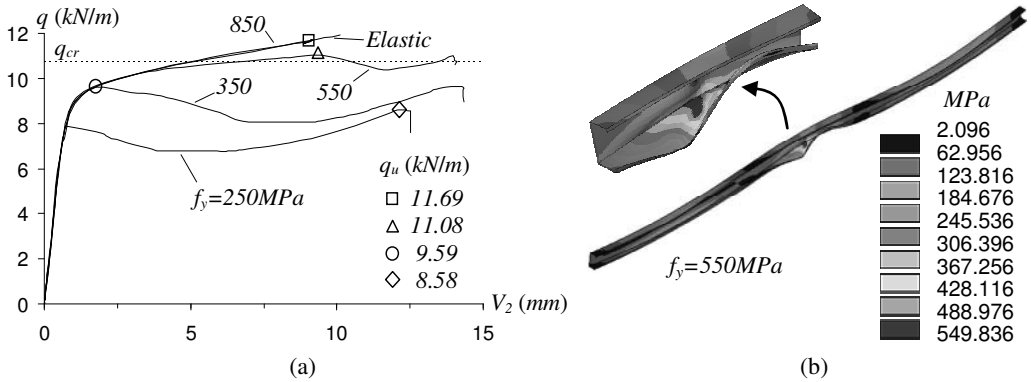

Figure 6: B8 beam (a) equilibrium paths and (b) deformed configuration and von Mises stresses at collapse.

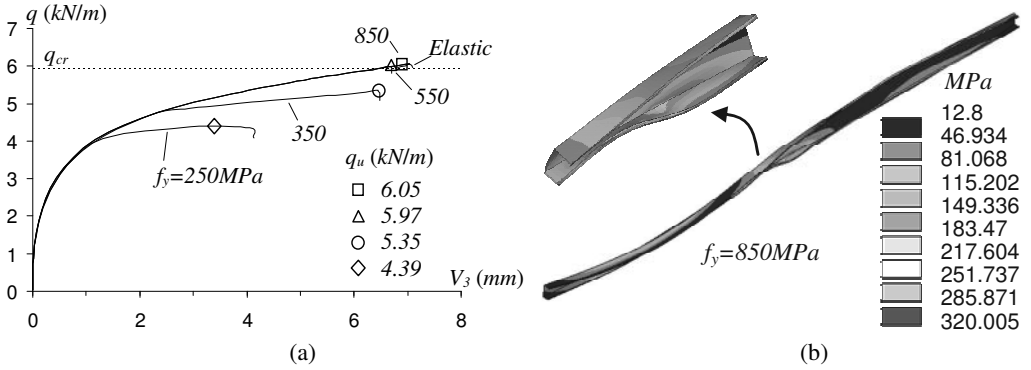

Figure 7: B10 beam (a) equilibrium paths and (b) deformed configuration and von Mises stresses at collapse.

The analysis of the post-buckling results presented in figures 5 to 7 leads to the following conclusions:

(i) The amount of post-critical strength reserve increases as (i_1) the yield stress increases (obviously) and (i_2) one "travels" from the B10 beams to the B4 ones, due to the growing presence of local buckling. The higher post-critical strength reserve occurs for the B4 beam with f_y=*850MPa* – ultimate-to-critical load ratio equal to *1.25*.

(ii) The bending moment redistribution is very clear in the beams with low yield stresses, whose collapse is less affected by the geometrically non-linear (buckling) effects. Figure 5(c) shows the deformed configurations of the B4 beam with f_y=*250MPa* associated with (ii_1) the full yielding of the intermediate support cross-section, occurring for *q=33.38kN/m* (point **I**), and (ii_2) the beam collapse, occurring for *q=37.75kN/m* (point **II**) and corresponding to the nearly simultaneously yielding of cross-section near the mid-spans.

(iii) The failure mechanisms of the beams with high yield stresses are very similar to corresponding critical buckling modes, thus implying that the collapse stems mainly from geometrically non-linear effects. Moreover, it is worth noting that the failures of all the beams with f_y=*850MPa* occur practically in the elastic range.

(iv) Increasing the yield stresses from *250MPa* to *850MPa* leads to ultimate load increases of *55.5%* (B4 beams), *36.2%* (B8 beams) and *37.8%* (B10 beams).

3 DSM DESIGN PROCEDURE

The DSM adopts "Winter-type" design curves, calibrated against experimental and numerical results concerning the ultimate strength of isolated (single-span) members acted by uniform internal force/moment. In beams, the nominal bending strengths against local (M_{nl}), distortional (M_{nd}) and global (M_{ne}) failures are given by the expressions

$$M_{nl} = M_y \qquad M_{nl} = \left(1 - 0.15\left(\frac{M_{crl}}{M_y}\right)^{0.4}\right)\left(\frac{M_{crl}}{M_y}\right)^{0.4} M_y \qquad (1)$$

$$(\lambda_l = \sqrt{M_y / M_{crl}} \le 0.776) \qquad (\lambda_l > 0.776)$$

$$M_{nd} = M_y \qquad M_{nd} = \left(1 - 0.22\left(\frac{M_{crd}}{M_y}\right)^{0.5}\right)\left(\frac{M_{crd}}{M_y}\right)^{0.5} M_y \qquad (2)$$

$$(\lambda_d = \sqrt{M_y / M_{crd}} \le 0.673) \qquad (\lambda_d > 0.673)$$

$$M_{ne} = M_y \qquad M_{ne} = \frac{10}{9}\left(1 - \frac{10M_y}{36M_{cre}}\right)M_y \qquad M_{ne} = M_{cre} \qquad , \quad (3)$$

$$(\lambda_e = \sqrt{M_y / M_{cre}} < 0.60) \qquad (0.60 \le \lambda_e \le 1.336) \qquad (\lambda_e > 1.336)$$

where (i) λ_l, λ_d and λ_e are *local*, *distortional* and *global* slenderness values, (ii) M_{crl}, M_{crd} and M_{cre} are the elastic global, local and distortional critical buckling moments and (iii) $M_y = W_y f_y$ is the cross-section first yield moment – W_y is the elastic modulus. In beams subjected to non-uniform bending, it is convenient to replace the various "M_y values" appearing in (1)-(3) by "first yield load parameter values" – in this case, the obvious choice is $q_y = 32M_y/L^2$.

It is worth noting that the application of expressions (1)-(3) corresponds to neglecting (i) the cross-section elastic-plastic strength reserve, in statically determinate or indeterminate beams, and (ii) the bending moment redistribution, in statically indeterminate beams – this means that overly conservative predictions are to be expected in statically indeterminate beams, particularly in the lower slenderness range.

Figures 8 to 10 show comparisons between the ultimate load predictions yielded by the current DSM design curves and the collapse loads obtained through SFE analyses involving B4, B8 and B10 beams with *15* different yield stresses, associated with yield-to-critical load ratios q_y/q_{cr} ranging from *0.06* to *3.74*. The numerical ultimate loads, normalised w.r.t. q_y, are represented by the symbols ○, □ and △, respectively for beam local (B4), distortional (B8) and global (B10) failures. Since the beams exhibit buckling and failure modes that are not "pure", the DSM curve choice was made on the basis of their "dominant buckling mode nature", given in table 1 – however, the λ_l, λ_d and λ_e are calculated with the actual beam critical buckling load q_{cr}, which is neither "purely" local, distortional or global. The observation of these comparisons prompts the following remarks:

(i) The DSM predictions are (i_1) excessively safe in the low slenderness range, (i_2) slightly safe in the intermediate slenderness range and (i_3) unsafe (local and distortional) or accurate (global) in the high slenderness range.

(ii) None of the DSM curves can predict efficiently (safely and economically) the two-span beam collapse loads, which is due to a combination of (ii_1) neglecting both the cross-section elastic-plastic strength reserve and (mostly) the bending moment redistribution (low slenderness range) and (ii_2) the "mixed" nature of the failure mechanisms (high slenderness range).

(iii) In the high slenderness range, the elastic critical buckling load curves (dashed lines) are either slightly below (B4) or passes right through (B8 and B10) the beam collapse load ratios.

(iv) Since the beam collapse loads already incorporate the local, distortional and global buckling effects, it seems to make little sense to neglect the cross-section elastic-plastic strength reserve and beam moment redistribution. The recent work by Shifferaw and Schafer [5] confirms this assertion – it reports experimental and numerical evidence, involving simply supported isolated beams (no moment redistribution), of the (logical) presence of a non-negligible inelastic strength in the low slenderness range.

(v) The most rational approach to account for the beam inelastic strength reserve (including moment redistribution) is to replace q_y (first yield loads) by q_{pl} (geometrically linear plastic collapse loads of the whole beam) in (1)-(3). Figures 8 to 10 also show comparisons between the ultimate load predictions yielded by these modified DSM design curves and the previous SFE collapse loads, now normalised w.r.t. q_{pl} and represented by the symbols ●, ■ and ▲. The observation of these new comparisons leads to the following comments:

(v.1) In the low slenderness range, the modified DSM predictions are either very accurate (local and distortional) or barely unsafe (global), which confirms the presence and relevance of the beam inelastic strength reserve.
(v.2) In the intermediate slenderness range, the modified DSM predictions are either accurate-to-unsafe (local and distortional) or clearly unsafe (global).
(v.3) In the high slenderness range, the modified DSM predictions practically coincide with the previous ones.

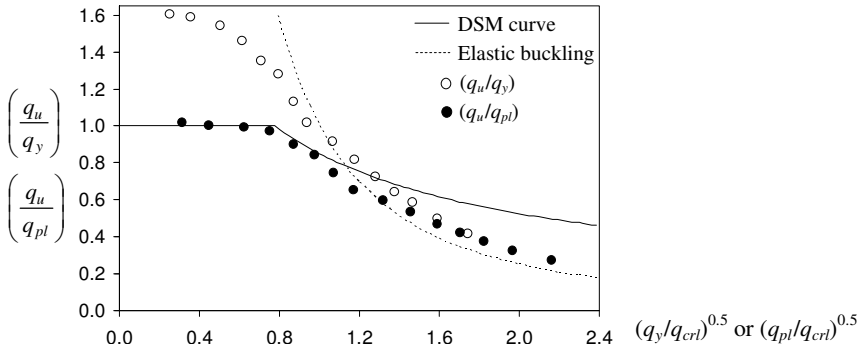

Figure 8: Comparison between SFE B4 beam collapse loads and DSM local design curve predictions.

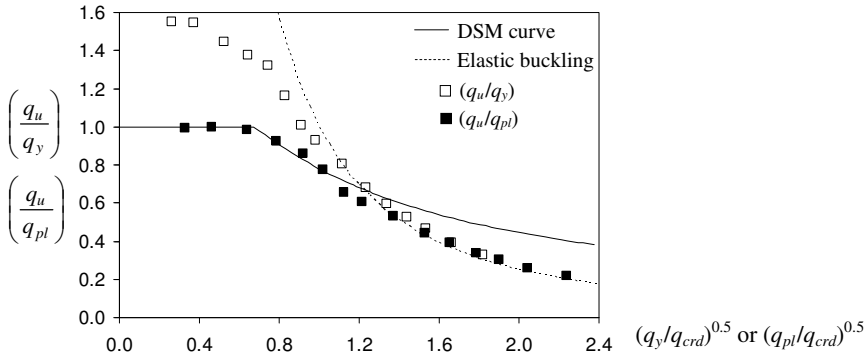

Figure 9: Comparison between SFE B8 beam collapse loads and DSM distortional design curve predictions.

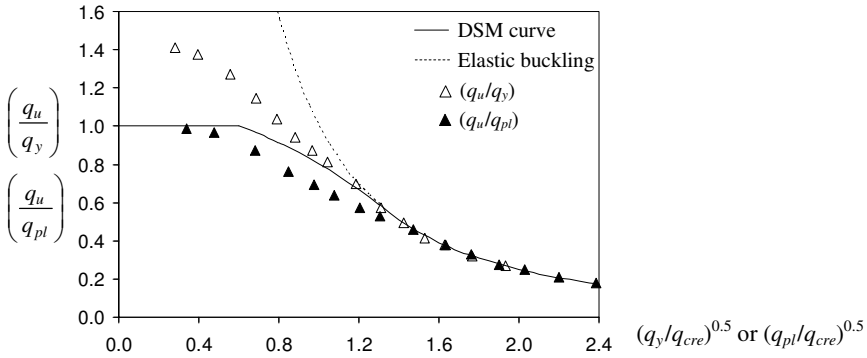

Figure 10: Comparison between SFE B10 beam collapse loads and DSM global design curve predictions.

Although much more research work is obviously needed before it is possible to have a firm opinion on the DSM design of multi-span cold-formed steel beam, it seems possible to make some preliminary comments on the basis of

the limited amount of results (both in quantity and in scope) presented in this work:

(i) Since there are no "pure" buckling and failure modes, the DSM curve choice should be based on the concept of "dominant buckling/failure mode nature".

(ii) The first yield load (moment) should be replaced by the first-order plastic collapse load (moment), thus accounting for the cross-section elastic-plastic strength reserve and beam moment redistribution. Failing to do this will inevitably lead to overly conservative prediction in the low slenderness range.

(iii) Apparently, the most rational approach is to develop and calibrate design curves that are based on (iii_1) the plastic collapse load, for stocky beams, and on (iii_2) the elastic buckling load, for slender beams. Nothing can yet be said about the intermediate slenderness range (or about the slenderness limits separating the three ranges) – nevertheless, the current DSM design curves provide the quite satisfactory ultimate load estimates in this range.

4 CONCLUSION

This work reported the results of an ongoing numerical investigation on the buckling, post-buckling, collapse and design of two-span cold-formed steel lipped channel beams subjected to uniformly distributed loads. These results consisted of (i) critical buckling loads and mode shapes, determined through GBT and ANSYS analyses, (ii) post-buckling equilibrium paths (up to collapse), deformed configurations and von Mises stress distributions, obtained by means of ANSYS elastic and elastic-plastic shell finite element analyses, and (iii) ultimate load predictions, yielded by the current DSM design curves. The following aspects deserve to be mentioned:

(i) The beam buckling and failure modes combine two or three types of deformation modes, which precludes a straightforward classification. Thus, one must resort to the "dominant buckling/failure mode nature" concept.

(ii) The beam post-buckling behaviour and inelastic strength reserve (ii_1) depend on the buckling/failure mode characteristics and yield-to-critical stress ratio, and (ii_2) may be heavily affected by moment redistribution, provided that the yield stress is low enough – on the other hand, failure may occur in the elastic range in beams with high yield stresses.

(iii) Due to the "mixed nature" of the beam failure modes, the choice of the appropriate DSM design curve (amongst the currently available ones) must also be based on the "dominant buckling/failure mode nature" concept.

(iv) The direct application of the current DSM design curves leads to either over-conservative (low slenderness) or clearly unsafe (high slenderness) beam ultimate load predictions.

(v) The numerical ultimate loads obtained clearly indicate that (v_1) the beams with low slenderness exhibit a fair amount of inelastic strength reserve, stemming mostly from the moment redistribution, and (v_2) ultimate loads of beams with high slenderness are fairly well approximated by their critical buckling loads, particularly if global buckling is involved. Although further studies are required to confirm these preliminary findings, it seems that the current DSM design curves will only be efficient if modified to take into account these two aspects.

ACKNOWLEDGEMENTS

The first author gratefully acknowledges the financial support provided by *"Fundação para a Ciência e Tecnologia"* (FCT – Portugal), through the post-doctoral scholarship nº SFRH/BPD/62904/2009.

REFERENCES

[1] Schafer B.W., "Review: the direct strength method of cold-formed steel member design", *Journal of Constructional Steel Research*, **64**(7-8), 766-778, 2008.

[2] Camotim D., Silvestre N., Basaglia C. and Bebiano R., "GBT-based buckling analysis of thin-walled members with non-standard support conditions", *Thin-Walled Structures*, **46**(7-9), 800-815, 2008.

[3] Yu C. and Schafer B.W., "Simulation of cold-formed steel beams in local and distortional buckling with applications to the direct strength method", *Journal of Constructional Steel Research*, **63**(5), 581-590, 2007.

[4] Swanson Analysis Systems Inc., *ANSYS Reference Manual* (version 8.1), 2004.

[5] Shifferaw Y. and Schafer B.W., "Inelastic bending capacity in cold-formed steel members", *Proceedings of Structural Stability Research Council Annual Stability Conference* (New Orleans, 18-21/4), 279-299, 2007.